Case Studies in Thermal Engineering 51 (2023) 103523

Contents lists available at ScienceDirect

Case Studies in Thermal Engineering

journal homepage: www.elsevier.com/locate/csite

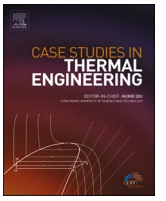

Ignition limit of EPS foam by a hot particle under cross wind

Supan Wang [a,b,**], Chunyin Zhang [a], Kaifeng Wang [a,b], Xinyan Huang [c,*]

[a] College of Safety Science and Engineering, Nanjing Tech University, Nanjing, China
[b] Institute of Fire Science and Engineering, Nanjing Tech University, Nanjing, 211816, China
[c] Department of Building Environment and Energy Engineering, Hong Kong Polytechnic University, Hong Kong, China

HIGHLIGHTS

- Airflow provides an alternative shortcut transition of unstable flash to a strong fire point.
- Airflow can increase the oxygen supply and flame heating rather than cooling the particle.
- Flash and fire points of hot-particle ignition were enhanced in the Smothering Regime.
- Flame retardants inside EPS foam do not change the flash ignition.
- Flame retardants inhibit the transition to fire point and burnout.

ARTICLE INFO

Keywords:
Building insulation materials
Fire point
Flash point
Flame-retardant
Spotting fire
Facade fire

ABSTRACT

The ignition of the building insulation materials by a hot particle is a typical spot fire phenomenon, but the scientific understanding is still limited. In this work, a hot steel spherical particle (6-16 mm and 800-1200 °C) was dropped onto the low-density expandable polystyrene (EPS) foam with an external airflow velocity of 0-4 m/s to obtain the ignition limit at the flash point and fire point. Airflow provides an alternative shortcut transition of unstable flash flame to a strong fire point and fuel burnout, because airflow increases the oxygen supply and flame heating rather than cooling the particle. As the airflow velocity increases, both flash and fire points first become easier to reach because airflow facilitates the mixing of pyrolysates and oxygen in the Smothering Regime. When the airflow velocity increases to the Thermal Regime, the delay time remains stable. Further increasing the airflow velocity to the Chemical Regime, the ignition delay time slightly increases until the airflow blows off the flash flame by cooling the particle or blowing away the flammable mixture from the hot surface. Such a competitive effect of airflow on hot particle ignition is also qualitatively verified by theoretical analysis. Flame retardants inside EPS foam do not change the flash ignition but inhibit the transition to fire point and burnout, even under the assistance of airflow. This work enhances the comprehension of the complex interactions between flash points and fire points in the spotting or hot-particle ignition of the building facades.

1. Introduction

To improve building energy efficiency, plastic insulation materials with low thermal conductivity, such as polystyrene, polyisocyanurate, and polyurethane, are extensively applied in building external insulation or façade, due to their low cost and superior

* Corresponding author.
** Corresponding author. College of Safety Science and Engineering, Nanjing Tech University, Nanjing, China.
E-mail addresses: wangsp@njtech.edu.cn (S. Wang), xy.huang@polyu.edu.hk (X. Huang).

https://doi.org/10.1016/j.csite.2023.103523
Received 26 August 2023; Received in revised form 19 September 2023; Accepted 22 September 2023
Available online 23 September 2023

insulating performance. Nevertheless, the flammability of these materials has long been a safety concern to its fire hazard [1–4]. Furthermore, compared with inorganic building insulation materials, these flammable materials are all easier to be ignited by hot particles produced during fireworks displays, electrical faults (Fig. 1a), or welding processes (Fig. 1b). In the last decade, several disastrous fires, such as the China Centre Television fire (2009) (Fig. 1c), the high-rise residential hall fire in Shanghai Jing'an district (2010) (Fig. 1d), and the New Zealand International Convention Centre Fire (2019), were triggered by the hot-particle ignition of external wall insulation [5]. The flash ignition of these materials by a hot particle has been commonly observed and does not result in the complete consumption of the foam sample in the laboratory [6–8]. However, in a real fire scene, the fire point is easy to reach to burn out the fuel. Thus, a big knowledge gap exists in the limiting condition of flash point and fire point over these insulation materials by a hot particle, and such information holds significant importance for enhancing building fire safety [7–11].

The ignition triggered by hot particles is fundamentally unlike the common radiation- or flame (convection)- driven ignition [7–10, 12–15]. These hot particles can serve as the heat source for fuel heating, and also the pilot source to initiate the ignition of the pyrolysis gases [9,16]. The buoyance-induced airflow by the hot particles will cool the inert/reactive particles or help the combustion of the reactive particles, and also affect the temperature and mixing process between the oxygen and pyrolysis gas. The hot-particle ignition propensity is dependent on the particles' state (material, molten, energy, size, temperature, etc.) [17–22], the fuel bed properties (composition, moisture, density, inclination, etc.) [7,23,24], the interactions between the particle and the fuel bed (splashing [22], bouncing, or extent of embedded into the fuel bed), and the environment (temperature, humidity, wind, etc.) [21,23,25,26]. The ignition processes of natural particles (e.g., burning firebrands and embers) are more complex than inert particles because they are reactive [16,27–33].

Previous work on the hot particle of building insulation materials showed that compared to temperature and size, the influence of the metal type (various thermal properties) and particle void ratio (mass and energy) was relatively weak, unless the particle made by the metal like some alloys and copper melt or had a large void ratio ($>$0.80) [8,12,18,19]. For tiny particles (diameter $<$ 8 mm), the minimum ignition temperature rapidly increased, as particle size decreased, due to small energy and fast cooling [12,19]. For large hot metal particles (diameter $>$8 mm), the minimum temperature initiating the hot-particle ignition of the expandable polystyrene (EPS foam) was about 800 °C, while the thickness and density of the sample had a small influence on hot-particle ignition [7]. The above studies mainly present a short-term flame, and do not result in the complete consumption of the foam sample, forming a small hole in the sample (i.e., flash ignition). The flash flame quickly disappears because the particle is not hot enough [7], or does not have adequate oxygen supply and a long particle residence time [8]. However, in a real fire scene, the fire point is easy to reach to burn out the fuel. Thus, there is a question, "*How could facilitate the transition from flash to fire point for hot-particle ignition*?"

All these previous studies of building insulation materials by hot particle ignition were conducted without environmental wind. However, the hot particle ignition in practice could be accompanied by environmental airflow and rising fire plumes. The effect of wind on hot-particle ignition has been studied previously for natural fuels [21,23,26]. The winds from 0 to 4 m/s promote direct flaming and smouldering ignition, and smouldering is more prone to flaming transition [23]. Wind can not only assist in the continuous ignition of the fuel (i.e., fire spread) [34,35] but also can cool the particle before ignition [23,36,37]. The experimental results on the hot-particle ignition of pine needles indicate that the particle cooling effect by wind (0 to 4 m/s) is less pronounced compared to the

Fig. 1. Hot particles generated by (a) electrical fault and (b) welding processes (Credit: tornadochaser66), and disastrous fires of (c) China Centre Television fire (2009) (Photo courtesy Wiki Commons) and (d) Shanghai high-rise residential hall fire in 2010 caused by hot particles (Credit: Shine).

concurrent augmentation in fuel heating [23]. This double-edged effect of wind leads to the question, "*Does external airflow intensify or mitigate the risk of spotting fire hazards for building insulation materials*"?

Flame-retardant (FR) treatment is widely used for insulation materials like EPS in the building to improve fire safety. The Class-B1 FR-EPS foam in China is widely used as an excellent flame-retardant and smoke-suppressant performance [38], and presents a lower limiting oxygen index and smoking density rate than normal fuel without flame retardant processing [39–41]. It can be judged that the FR materials are still combustible, even present a more susceptible to smouldering in oxygen-enriched environments [41], and are more likely to transition to a flaming fire [42]. For normal EPS foams, sufficient flammable fuel can be pyrolysed within a short period, and the hot-particle ignition of these plastic foams was governed by the competition between the particle residence time and the gas mixing time [7]. So far, *the impact of FR treatment on preventing spotting ignition and subsequent fire spread is unclear*, presenting a gap in our knowledge.

The spotting ignition of normal and FR EPS foam induced by a single steel particle under various airflows has been investigated in this work. A short-term flame (i.e., flash point), a sustained flame that burnt out the fuel (i.e., fire point) and no ignition are captured and described in detail. This work systematically quantifies the ignition limits of flash and fire points, relating to the airflow velocity, the diameter, temperature, and void ratios of the particles, and normal and FR EPS foam. The ignition delay time was measured and analysed to understand the complex airflow effect on the hot-particle ignition. Afterwards, the competitive effect of airflow on hot particle ignition is also discussed qualitatively by using fundamental theories on mass and heat transfer. This knowledge is essential for predicting and managing fire hazards more effectively.

2. Experimental methods

2.1. EPS fuel bed and particle

To facilitate comparison with the literature [6–8], this work follows the previous experiments of the normal and FR EPS foams as representative building insulation materials. Herin, EPS is made by catalytic polymerization of styrene. And the FR EPS foams were FR Class B1 (GB 8624-2012, Chinese Standard), which has a Fire Growth Rate (FIGRA [43]) of $FIGRA_{0.2MJ} \leq 120$ W/s or $FIGRA_{0.4MJ} \leq 250$ W/s. Here, the defined FIGRA is always the maximum ratio of the heat release rate (i.e., the subscription) to the burning duration. The measured densities of normal and FR EPS foam in the experiment were 18.4 ± 0.4 kg/m^3 and 19.9 ± 0.4 kg/m^3, respectively.

A cuboid EPS sample with a 200 mm × 200 mm cross-section and 50 mm thickness was selected to sufficiently capture the ignition and flame spread processes. To minimise heat loss and oxygen leakage from the sides and bottom, four sides of the sample were covered by fireproof asbestos and aluminium foil, and the bottom was placed on the fireproof board.

The experiments chose spherical steel particles with various diameters (D, 6 - 16 mm) and void ratios (e, 0 - 0.8), which mimicked the porous metal particles generated from actual welding or firework processes. The hollow particle was specially made by welding two steel shell hemispheres (the shell thickness is 0.6 mm), the production method and more details can be found in the previous study [8]. Since Bi value of the particles was quite small ($Bi \approx 0.02 < 0.1$ [44]), there was a uniform distribution of temperature inside the particle during the entire heating and ignition processes.

2.2. Experimental setup

The experimental setup of hot particle ignition, which mainly consisted of a tubular furnace, an airflow supply system, and a fuel bed, is presented in Fig. 2. It consisted of a tubular furnace (SK 2-2.5-13 TS, 0–2.5 kW) to heat the metal particle, and the heating power control system to regulate the furnace temperature. The furnace was heated by silicon carbide heating elements to a pre-set temperature (800-1300 °C), and regulated by a Type-S (platinum-rhodium) thermocouple and the control system [6–8]. To avoid the influence of the particles' verticle momentum, the tube outlet of the furnace rested on the top surface of the EPS foam.

The airflow supply system was used to create a uniform environmental airflow for the experiment. In this setup, an axial flow fan

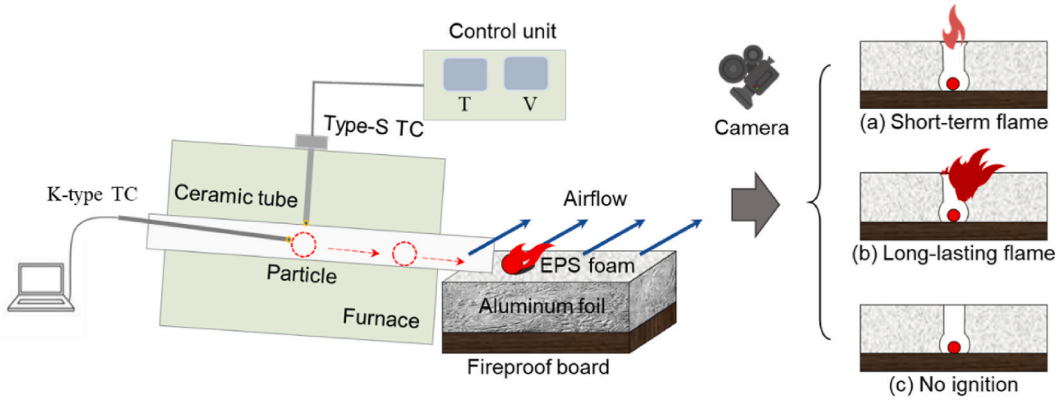

Fig. 2. The schematic diagram of the experimental setup and the main ignition phenomena for hot particle ignition of EPS foam.

(SF4-4 Type) is controlled by a power sensor with a frequency range of 0–50 Hz and 0.1 Hz resolution to provide the desired external airflow (from 0 to 4 m/s) at the leading edge of the sample. To homogenize the flow, a 2 m-long fairing was placed after the outlet of the fan [45]. To explore the impact of airflow on hot-particle ignition, the experiments were conducted under the airflow velocities U_a from 0 (no-wind) to 4 m/s, that is much larger than the particle's horizontal moving speed of 0.28 ± 0.05 m/s.

2.3. Procedures and measurements

Before the experiment, the centre-line airflow velocity at the forefront of the sample was measured with a handheld anemometer, ranging from 0 to 30 (±0.01) m/s. The particle was introduced into the centre of the furnace, once the furnace temperature was stabilized. The surface temperature of the particle was calibrated by a K-type thermocouple (0.5 mm), which would be quickly raised and stabilized to a pre-set temperature (T_p) [7,8]. Once the particle temperature achieved a consistent and uniform value, the particle was gently released to roll down along the ceramic tube. The particle temperature during the dropping procedure is difficult to monitor, so the initial parameter (hot particle temperature) at the released point was controlled. Here the experiment was designed to have a minimum particle bounce or residence time in the airflow and avoid the airflow cooling of particles.

The time history of motion, ignition, and fire spread processes was captured by two digital video cameras at 50 frames per second from a 45° bird's-eye view and a front view. For each scenario, at least 5-10 repeating test runs were conducted to quantify the ignition probability and ensure the repeatability of experimental outcomes.

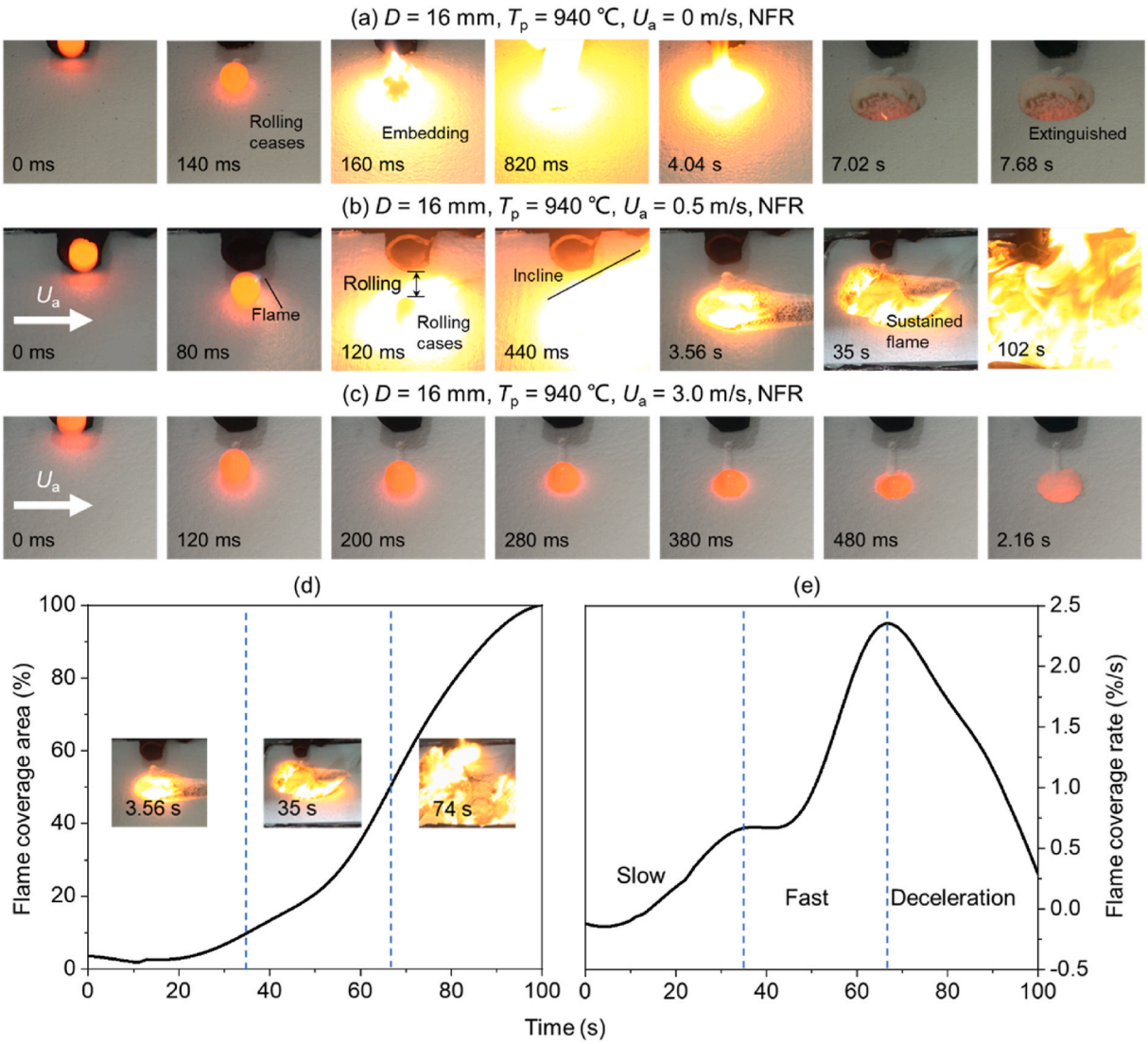

Fig. 3. Snapshots of typical (a) flash point ignition, (b) fire point ignition, and (c) no ignition processes with the hot particle (solid, D = 16 mm, 940 °C) igniting normal EPS foam at different airflow velocities: (a) U_a = 0 m/s, (b) U_a = 0.5 m/s, and (c) U_a = 3 m/s. (d) Flame coverage area and (e) coverage rate for U_a = 0.5 m/s.

3. Experimental results

3.1. Flaming ignition phenomena

Fig. 3 illustrates typical (a) flash point ignition with a short-term flame, (b) fire point ignition with a long-lasting flame, and (c) no ignition processes from the 45° bird's-eye camera, with normal EPS foam and a 16 mm solid particle (940 °C) at various wind speeds of 0, 0.5, and 3 m/s (Supplementary Videos S1-3 for original videos). There was no occurrence of smouldering ignition due to extremely little char generated from the pyrolysis of EPS foam. The moving and ignition processes of the hot particle can be obtained from the main view, which is the same as the past findings [6–8] and not presented here. Herein, the time zero was set to the moment that a heated particle landed on the target sample surface. In no-wind conditions, the ignition processes are similar to our previous experiments [7,8]. As shown in Fig. 3a, the moving particle rolled horizontally about 2-8 cm to stop rolling over the fuel surface at 140 ms, and began to be gradually embedded into the sample. A strong pre-mixed flame surrounded the particle immediately at 160 ms (called embedding ignition in Ref. [7]). Then, the flame could quickly transition to the diffusion flame, and the particle was gradually embedded until the fireproof board. This entire penetration process lasted about 1 s. Afterwards, the flame gradually diminished and ultimately extinguished at 7.68 s.

By adding a 0.5 m/s horizontal airflow see Fig. 3b, the flame first appeared on the downwind side at 80 ms while the particle was still rolling horizontally over the fuel bed surface. Such an ignition is called the "rolling ignition", as previously defined in Ref. [7]. Then, the particle stopped rolling at 120 ms. During the particle embedding in the target sample, the flame started to cover the sample surface and had a steady incline at 440 ms. The weak flame around this hot particle, continuously heated the fuel bed. Since 3.56 s, the flame no longer remained on the sample surface, but entered the hole penetrated by the hot particle, gradually reaching the "fire point". A clear charred area and a large cave on the fuel bed surface were generated by the strong flame.

Supplementary video related to this article can be found at https://doi.org/10.1016/j.csite.2023.103523

The area covered by the flame on the fuel bed surface and its flame spread rate was obtained and presented in Fig. 3d-e. During 0 -

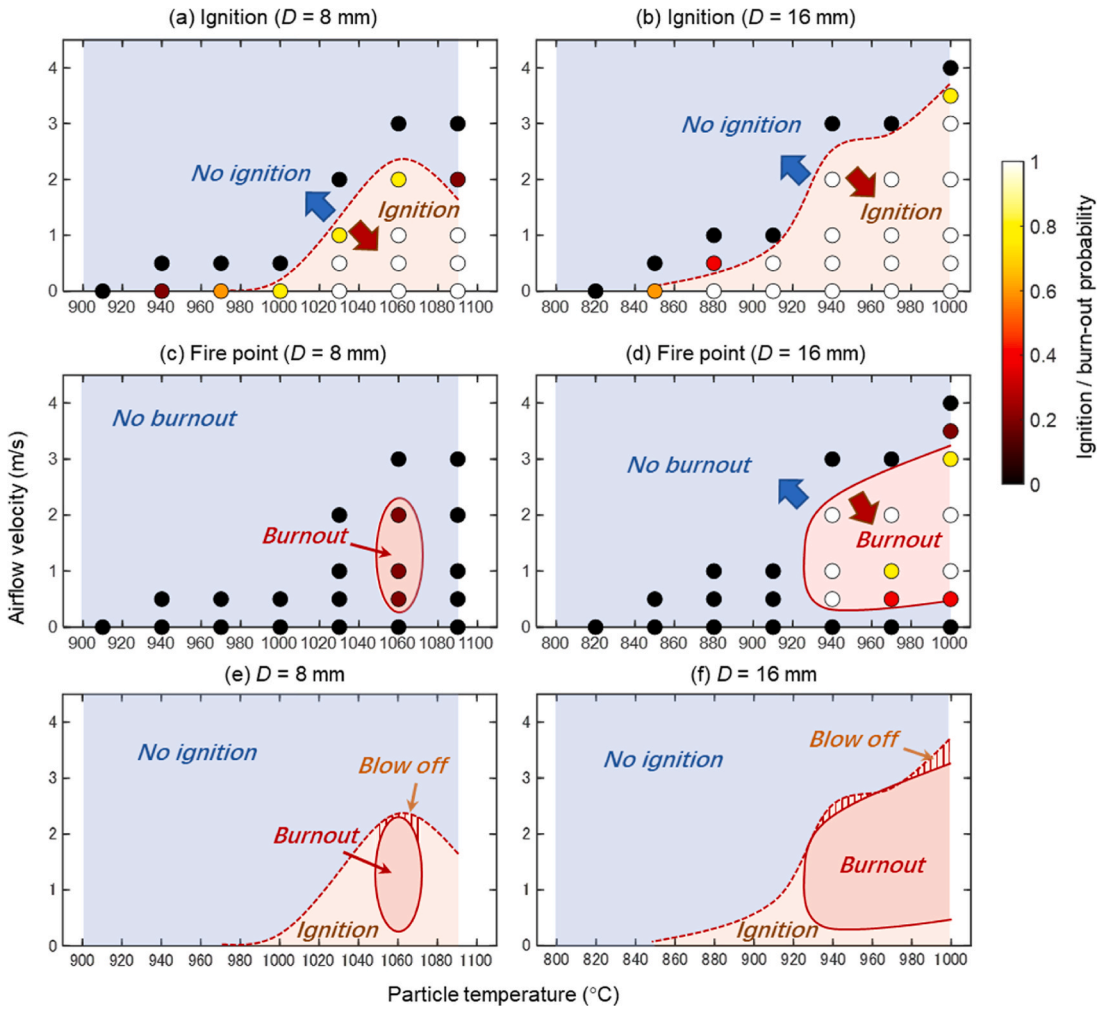

Fig. 4. Ignition and burnout probability, as a function of the airflow velocity, and the diameter and initial temperature of the hot particle, for normal EPS foam.

35 s, the flame front advanced slowly and mainly in the hole. Afterwards, the flame started to spread on the surface as seen at 35 s. At about 35 - 65 s, the flame spread rate rapidly increased as the hole's diameter expanded. When the flame advanced about 50% range of the fuel, the spread rate gradually slowed down until it completely covered the fuel bed. This is a two-dimensional and complex fire-spreading process, and thus deserves a dedicated investigation in future work. It is attributed that the convective heat transfer from the direct flame to the fuel bed in the wind-aided case is stronger than in the no-wind condition. The flame eventually burnt out the entire EPS sample at around 102 s. Thus, the wind can extend the hot-particle ignition limit [7] after the hot particle lands on the fuel bed. In other words, airflow offers an alternative shortcut to attain the fire point. In the absence of airflow, the particle temperature needs to elevate by an additional 100–200 °C to reach the fire point, which is above 1100 °C [7]. Note that before the contact, the wind is cooling the hot particle.

By adding a 3 m/s horizontal airflow see Fig. 3c, the hot particle ignition did not occur for the same particle and fuel bed as Fig. 3a and b. Herein, the processes of rolling and descending resembled the ignition case, but no smoke or flame was observed. The wind effect, perhaps cooling or blowing away of pyrolysates becomes dominant, which suppresses the hot particle to initiate a piloted ignition.

3.2. Flash and fire points of EPS foam by a hot particle

To quantify the various ignition phenomena, the presence of a visible flame that can be sustained for longer than 1 s is defined as successful ignition, which contains "flash point" and "fire point" ignition. In this work, the successful ignition is considered as the flash point. If the flame can completely burn out the fuel, it will be further considered as the fire point. Therefore, the flash point encompasses both brief and stable flame cases, while the fire point specifically refers to the case of the stable flame. Based on the previous work [7,8,23], ignition probability (P_{ig}) can be the ratio of successful ignition (N_{ig}) to the repetition (N_{tot}) as

$$P_{ig} = \frac{N_{ig}}{N_{tot}} \times 100\% \tag{1a}$$

Similarly, the probability of a "fire point" (P_{fire}) can be defined as the ratio of successful burnout (N_b) to the repetition (N_{tot}) as

$$P_{fire} = \frac{N_b}{N_{tot}} \times 100\% \tag{1b}$$

Fig. 4 compares the probability distribution of ignition and fire point at different solid hot-particle temperatures (T_p), diameters (D), and airflow velocities (U_a) for normal EPS samples. Each coloured circle represents at least 5 repeat runs, and the ignition (P_{ig}) or burnout (P_{fire}) probability is scaled by the colour bar from 0% (black) to 100% (white). To simplify a comparison, the critical airflow velocities at $P_{ig} = 50\%$ and $P_{fire} = 50\%$ were plotted.

As expected, the burnout (fire point) of the EPS foam is much more difficult than that of "flashpoint" ignition (see more comparisons in Fig. 4e-f). The particles of two sizes exhibit a comparable trend: for a higher particle temperature, a wider airflow limit was perceived for ignition and burnout. For instance, to ignite EPS foam with a 16 mm particle diameter and 50% ignition probability, the upper airflow limit is around 3.5 m/s with particles of 1000 °C, seven folded that with particles of 880 °C. On the other hand, if the particle temperature is raised from 940 to 1000 °C with a 16 mm particle diameter, the airflow limit of burning out the EPS foam, will increase by one time from 0.5 to 2.0 m/s to 0.5–3.5 m/s. And as the airflow velocity increases, the flash ignition probability decreases, when the particle temperature is close to the critical temperature. But the airflow velocity has a negligible influence on the flash ignition probability when the temperature of the particle is much hotter than the critical temperature of flash ignition. Above the critical wind of the fire point, flaming extinction or blow-off will occur by increasing the airflow velocity. In the theoretical, this external airflow can inevitably make piloted ignition by hot particles more difficult.

Moreover, both particle temperature and wind are not sufficient conditions to reach the fire point of the sample. As illustrated for the 8-mm particle size in Fig. 4c, the particles of 1060 °C have reached the fire point at 0.5–2.0 m/s wind, but the fire point has not been

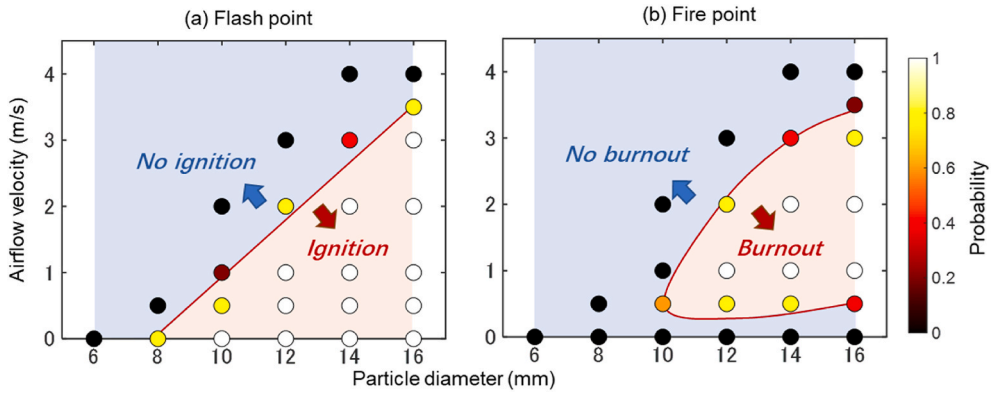

Fig. 5. (a) Ignition and (b) burnout probability for normal EPS foam as a function of the diameter of hot particle and airflow velocity at 1000 °C.

reached for that of 1090 °C. For a 16-mm particle (1000 °C), the flame that remained on the sample surface for 3.5 m/s wind (similar to flash point ignition in Fig. 3a) is more unstable and easily blows off than that of 3 m/s wind. The in-depth analysis found that the flame residence time on the sample surface for 3.5 m/s wind was half that of the 3 m/s wind case. It is reasonable because the molten EPS, without enough pre-heating from the existing flame, cannot maintain sustained pyrolysis. Thus, the fire point requires sufficient particle temperature, airflow-aided, and a longer hot-particle flash duration.

Comparatively, the airflow limits of ignition and fire point are quite different between the particle size of 8 mm and 16 mm, suggesting a strong particle size dependence for ignition under the tested particle temperature. The above large dependence on particle size has also been observed for the hot-particle ignition by solid and hollow particles [8]. Fig. 5 further illustrates the boundary of hot-particle ignition and burnout, as a function of airflow velocity (U_a) and the particle diameter (D), with a particle temperature of 1000 °C. As the particle size increased, it was easier to achieve the ignition or burnout of the EPS foam, especially under the immediate airflow. For the ignition boundary (Fig. 5a), the limiting airflow velocity also linearly increases with the increasing particle size. Fig. 5b shows that if the external airflow velocity is between the upper and lower curve limits, the sample has a notable risk to be burnout. While the fire risk is low, if the airflow velocity is outside the limit curve.

3.3. Flaming ignition delay time

The flaming ignition delay time (t_{ig}) can be quantified as the duration from the particle's landing ($t = 0$) and the emergence of the flame. Fig. 6 summarises the ignition delay time t_{ig} with various airflow velocities U_a and particle temperatures T_p for the particle sizes of 16 mm and 8 mm. Every data point represents the mean value of 5–10 repeat runs, and the error bar is the standard deviation. A similar trend is found for the tested particle size range. That is, as the airflow velocity increases, this ignition delay time first reduces to a minimum value (Smothering Regime) and then stays almost the same across a broad spectrum of airflow velocities (Thermal Regime). Subsequently, the ignition delay time slightly increases (Chemical Regime) until there is no ignition, following a similar pattern of the classical pilot ignition [46,47] and flame spread [48,49] for a solid combustible.

In a small airflow velocity (i.e., $U_a \approx 0.5$ m/s), the embedding ignition may transition to the rolling ignition (see more in Fig. 3a and b), which requires a higher critical temperature than that of embedding ignition in no-wind conditions [7]. Therefore, wind boosts heat convection between particles and fuel, and oxygen supply governs the hot particle ignition in the regime, while the cooling effect of airflow on particles is negligible. For instance, when the airflow velocity increases from 0 m/s to 0.5 m/s, the ignition delay time of the 16-mm particle (1000 °C) decreases monotonically from 80 ± 16 ms to 44 ± 8 ms. This increasing pattern is categorized as the Smothering Regime, a term commonly used in the context of the opposed flame spread [48,49].

With a continuous increase in the airflow velocity, the ignition delay time stabilises. For instance, the ignition delay time of the 16-mm particle (1000 °C) remains at 48.3 ± 9.8 ms as the U_a increases from 0.5 m/s to 2.0 m/s in Fig. 3a. For the wide-wind regime, this sufficient oxygen supply does not affect the ignition delay time. While the dominance of the ignition delay time shifts towards the thermal convection and conduction between the particle and the flammable gaseous mixture. This shift resembles the Thermal Regime of flame propagation, where the flame spread rate is controlled by the preheating of the flame [49].

Further raising the airflow velocity, the ignition delay time eventually begins to increase. This occurs because blowing away the pyrolysis gas or the cooling effect of external airflow on the pyrolysate-oxidation reaction (see Fig. 3b and d) can no longer be ignored. Therefore, the flaming ignition is governed by the competition between the cooling of the environment and the heat generation of the pyrolysate-oxidation reaction. Analogous to the piloted ignition or flame spread, such an ignition phenomenon is defined as the Chemical Regime [50]. Consequently, as the airflow intensifies, the convective cooling, or blowing away of the pyrolysis gas and oxygen, results in a deceleration of the pyrolysate-oxidation reaction. Ultimately, the cooling rate of airflow would equal or surpass the heat release rate from the pyrolysate-oxidation reaction, so no hot-particle ignition by airflow occurs. Noticeably, a large error in the ignition delay time with 16 mm particle (1000 °C) and $U_a \geq 3$ m/s, is attributed to the transition of hot-particle ignition phenomena from the rolling ignition ($U_a < 2$ m/s) to the embedding ignition ($U_a = 3.5$ m/s).

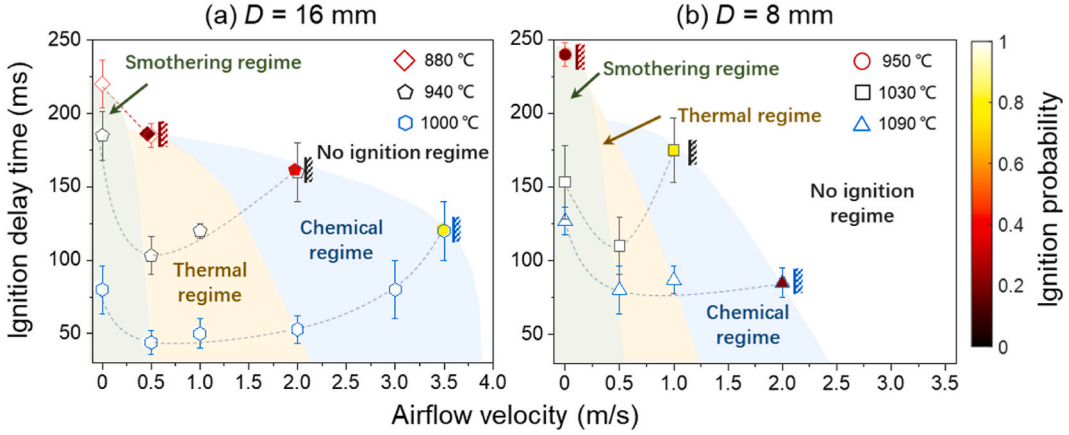

Fig. 6. Ignition delay time of normal EPS foam by a hot particle at various temperatures and airflow velocities: (a) $D = 16$ mm, (b) $D = 8$ mm.

According to the ignition delay time (t_{ig}), the influence of airflow velocities will first promote and then weaken the hot particle ignition under constant particle conditions (containing particle temperature and size). However, the best ventilation velocity (corresponding to the minimum t_{ig}) should be changed with the fixed particle conditions. When the particle temperature is equal to or lower than the corresponding critical temperature (P_{ig} = 50%), even 0.5 m/s wind will weaken the hot particle ignition from flash ignition to no ignition, such as the lower particle temperature (850 °C for 16 mm particle) in Figs. 4b and 6a.

For the hot-particle ignition of EPS foam in the wind, the particles still serve as the hot source of heating and pilot. Herein, the ignition time is analogous to the piloted ignition time of the radiation ignition process. In this context, the relationship of various particle temperatures (analogous to radiation heat flux) and ignition time, seems similar to the connection between the critical heat flux and radiation ignition time [51].

3.4. The cooling effect of external airflow on hot particle

To further assess the cooling impact of airflow on the hot particle, the hollow particles with $D = 16$ mm, and $e = 0.8$ were also tested under external airflow. Fig. 7a and b illustrate the probability distribution of ignition and fire point versus the hollow ($e = 0.8$) hot-particle temperature (T_p) and airflow velocity (U_a) for normal EPS samples. For ease of comparison, the second row features the replotting of critical airflow velocity (U_a) with 50% ignition or burnout probability for solid and hollow particles.

Here, the energy (E) [8] of the particle in Fig. 7c-d, mainly affected by the particle mass and temperature, can be defined as

$$E = mc_p(T_p - T_a) = e\rho_s\left(\frac{\pi}{6}D^3\right)c_p(T_p - T_a) \tag{2}$$

As the particle temperature increases, the critical airflow velocity of hollow particles to pilot a flame is first higher than (≤940 °C), then equal to (940 °C < T_p ≤ 970 °C) that of solid particles.

For example with the particle temperature of 910 °C and airflow velocities of 1 m/s, the ignition probability of a hollow (e = 0.8, 1.81 kJ) particle is 100% and much higher than that of a solid particle (8.82 kJ), which is against our intuition. In conclusion, if the particle is hollow,

(i) *It is not feasible to establish a critical particle energy for ignition,* and
(ii) Lower particle energy does not indeed indicate a lower risk of spotting fire.

In other words, in addition to particle temperature and energy, the interactions between the moving hot particle and the sample are the third determinant. The stronger ignition ability of the hollow particle (≤970 °C) is attributed to the longer residence of the hot particle to effectively increase the heating time [8]. Under external airflow, the mass nor energy of the particle is inadequate to quantify the hot-particle ignition limit or the spotting hazards, which is the same as the no-wind condition [8].

As the particle temperature is 1000 °C, the critical airflow velocity of hollow particles to pilot a flame is lower than that of solid particles. It is attributed that for a hollow particle, the corresponding ignition delay time is five times larger than that of a solid particle. The higher temperature decreases the residence time, but the particle is hot enough to pilot the pyrolysis gases. It can be proved by an

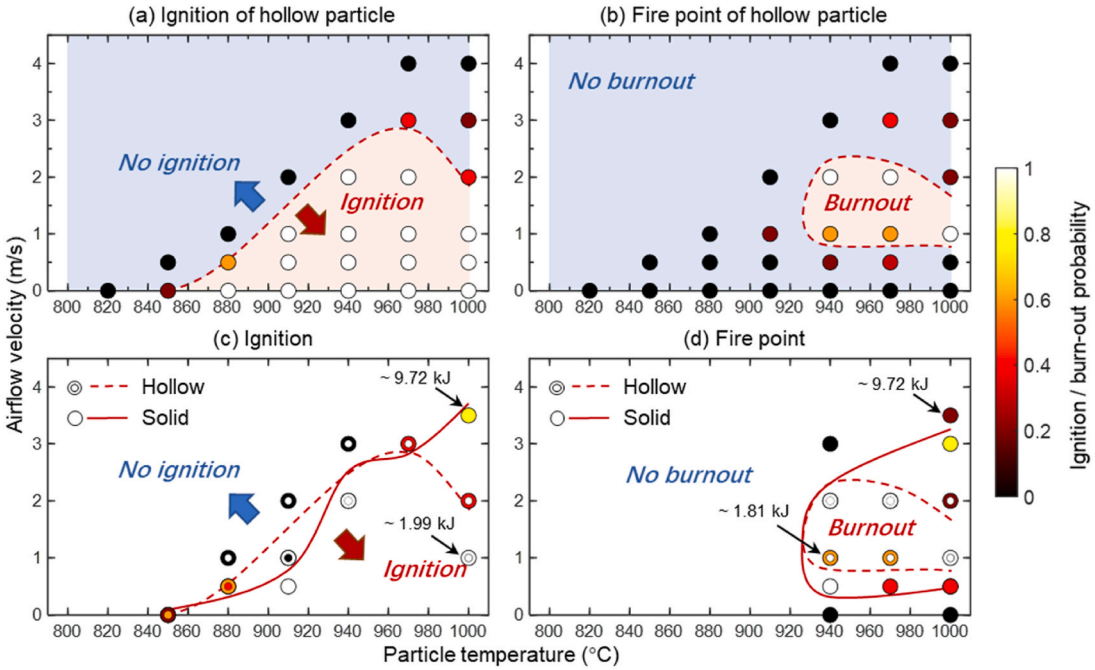

Fig. 7. Ignition and burnout probability as a function of the initial temperature and airflow velocity for normal EPS foam and hot hollow particle (e = 0.8).

unstable flash at 1.34 s in Fig. 8, where the particle was already embedded into the sample. Fig. 8 and Video S4 present a no-ignition case using the same particle temperature, fuel bed, and airflow velocity, but with a 0.80 void ratio with Fig. 3c. The intermittent flash vanished at 2.92 s, indicating a failed ignition.

Supplementary video related to this article can be found at https://doi.org/10.1016/j.csite.2023.103523

From the kinematics analysis [8], as the particle temperature decreases or the void ratio increases, the residence time of the hot particle increases, which means a very long cooling time. The appearance of an unstable flash is common for the hollow particle and confirmed that the hot particle, even accompanied by 3 m/s wind (strong cooling effect) and 0.80 void ratio (the particle shell is very thin), can still be hot enough to pilot the pyrolysis gases, regardless of cooling effects in current experiments. Further, increasing airflow velocity can lower the formation of the flammable mixture, which may be the dominant factor in reducing the fire risk of hot-particle ignition.

However, the fire point is more sensitive to solid or hollow particles than the flash point. Due to the smaller thermal inertia than solid particles, a hollow particle is more difficult to burn out the fuel bed, even at a higher temperature and airflow velocity (such as $T_p = 1000$ °C, $U_a \geq 2$ m/s), as presented in Fig. 7d. After the particle vertically penetrates the foam to the bottom, the reducing pyrolysis gas produced by thermal radiation from the particle cannot sustain the flame to reach the fire point. Therefore, the sustained energy supply of the solid particle would also affect the burnout limit.

3.5. Effect of flame retardant processing

Fig. 9 illustrates the typical hot-particle ignition process of FR samples under 0 and 0.5 m/s wind with $e = 0$, $D = 16$ mm, and $T_p = 940$ °C. Hot-particle ignition phenomenon of FR EPS foam and ignition delay time was similar to normal EPS foam and our previous work [7,8]. However, the flash duration of the normal samples is around two times longer than that of FR EPS foam. The flash flame cannot burn out the fuel for the FR EPS foam, even under the wind speed of 0.5 m/s in Fig. 9b.

Fig. 10 shows the FR effect on the observed probability distribution of ignition and fire point with the different solid hot-particle temperatures (T_p), diameters (D), and airflow velocities (U_a). As expected, under the same airflow velocity, FR EPS has a slightly higher temperature than that of normal fuel beds. As the particle temperature increases, the critical airflow velocity of FR EPS is lower than that of normal samples. For example, as the particle temperature increases from 880 °C to 970 °C, the critical airflow velocities increase from 0 m/s to 2 m/s for FR EPS foam and from 0.5 m/s to 3 m/s for normal EPS foam, respectively. The hot particle cannot ignite the FR EPS foam, when the wind speed exceeds 2 m/s. This occurs because higher airflow velocities reduce the effective concentration of the flammable pyrolysate, which acts as a resistance to fuel-gas mass transfer.

FR EPS foam is formed by catalytic polymerization of the styrene with flame retardant. With enriched flame retardants at the interfaces among the EPS beads [52], the FR samples will produce carbonaceous matter and form a protective layer to encapsulate the polymer matrix while being ignited. Naturally, the protective layer blocks the exchange channels of oxygen and pyrolysis gases to extinct the flash flame. Meanwhile, compared with normal EPS foam, the flame of FR EPS samples was generally easily extinguished without burnout of the fuel, even in all airflow velocities and particle conditions in Fig. 10b.

To further evaluate the FR effect on the hot particle ignition, Fig. 11 presents the observed distribution of ignition probability versus the particle's initial temperature (T_p) and diameter (D) for normal and FR EPS foam in no-wind conditions. For the sake of comparison, the critical hot-particle ignition temperature at $P_{ig} = 50\%$ was selected. Both normal and FR samples exhibit a comparable trend: hot-particle ignition of a smaller particle requires a higher temperature. For instance, to achieve a 50% probability of igniting an FR EPS sample, as the particle diameter decreases from 16 to 4 mm, the critical particle temperature needs to increase from 1150 to 880 °C. There is a 30~60 °C temperature range for the transition region bounded by $P_{ig} = 5\%$ and 95%, similar for all particle sizes. A comparison between Figs. 11a and b shows very small differences between normal and FR EPS samples (less than 25 °C) in terms of critical ignition temperatures. This suggests a weak effect of flame retardant on hot-particle ignition under the currently tested particles. The weak dependence on flame retardant can be verified by the thermogravimetry curve of normal and FR EPS foam in Fig. A1.

4. Heat and mass transfer analysis

4.1. Airflow effect on the hot particle ignition

The particle still serves as the hot source of the heating and piloted ignition like a flame. In the case of piloted ignition by a hot inert particle,

$$t_{ig} = t_{py} + t_{mix} + t_{chem} \tag{3}$$

In no wind condition, strong pieces of evidence have proved that sufficient fuel is pyrolysed within a negligible time.

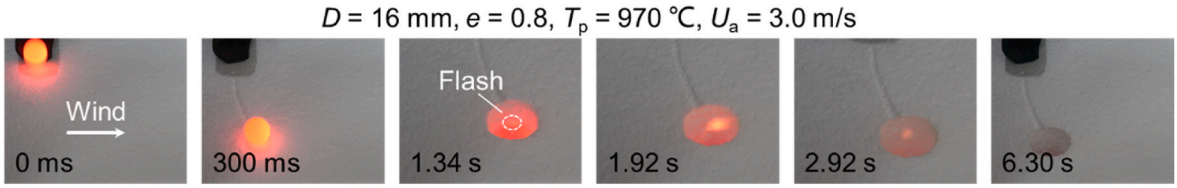

Fig. 8. Snapshots of the hot particle ($D = 16$ mm, $e = 0.8$, $T_p = 970$ °C) igniting normal EPS foam at a high airflow velocity ($U_a = 3$ m/s).

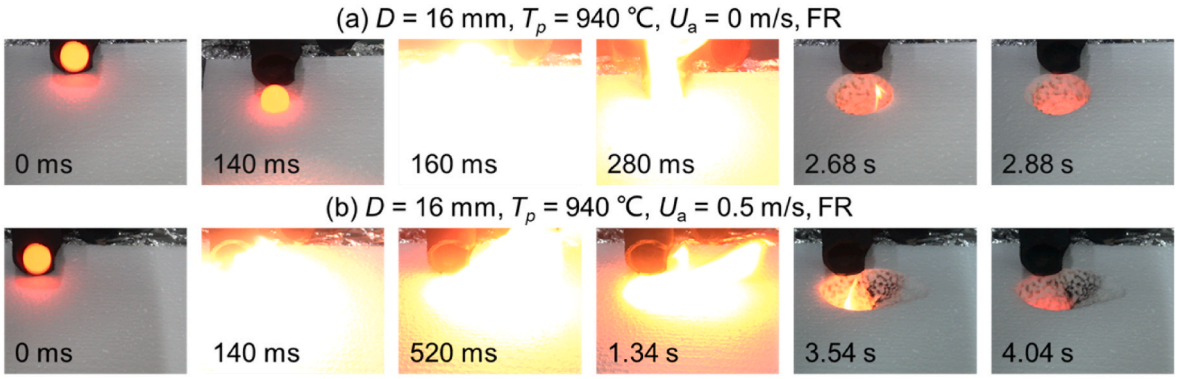

Fig. 9. Snapshots of the hot particle (D = 16 mm, solid, T_p = 940 °C) igniting FR EPS fuel bed (a) U_a = 0 m/s (b) U_a = 0.5 m/s.

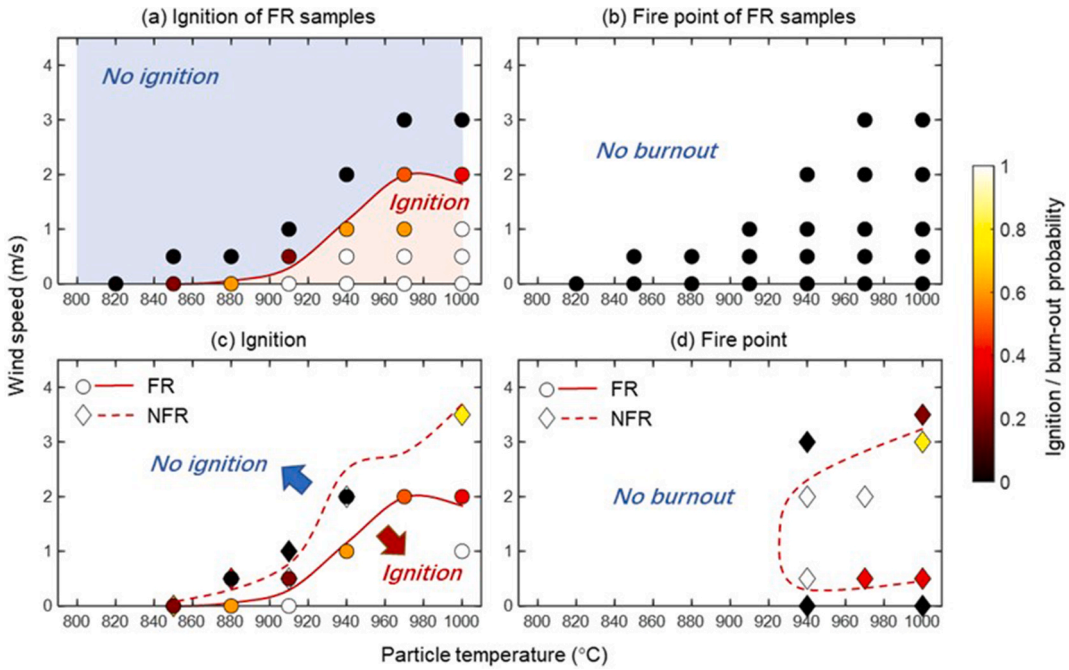

Fig. 10. (a) Ignition and (b) burnout probability for FR EPS foam as a function of airflow velocities and the initial temperature of a hot particle (D = 16 mm).

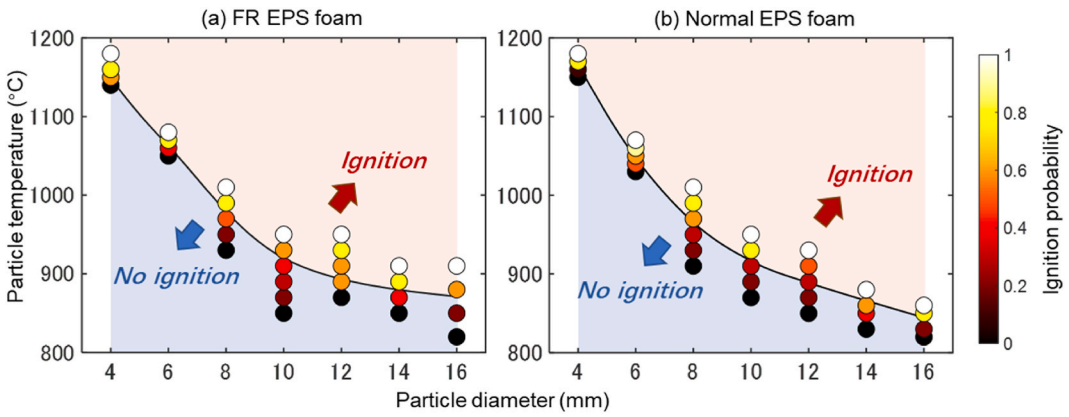

Fig. 11. Ignition probability of the (a) FR EPS foam and (b) normal EPS foam as a function of the initial diameter and temperature of hot particles.

1) The particle temperature (>800 °C) is much higher than the characteristic pyrolysis temperature of EPS foam (below 350 °C according to TGA), and it can be rapidly reached after the contact between the foam and hot particle.
2) The particle energy significantly exceeds the pyrolysis energy needed to achieve the lower flammability limit of the EPS foam.
3) There was a small and visible flame during the rolling and embedding processes of the particle.
4) The ignition temperature of the hot particle is independent of the foam density.

The ignition occurs when the mixing of the pyrolysate and air reaches the lower flammability limit, and the piloted ignition occurs inside the boundary layer of the particle. For the hot-particle piloted ignition on the top surface of the sample, the mixing time can be approximated by the fuel-gas diffusion time across the boundary layer on the particle [51] as

$$t_{mix} \sim \frac{\delta^2}{\alpha} \approx \frac{(D/Nu_D)^2}{\alpha} \tag{4}$$

where diffusivity (α) increases with the particle temperature and airflow velocity. Hence, as the particle temperature and airflow velocity increase, the mixing time decreases. Under a small external airflow, the gas-phase chemical duration is short, $O(10^{-4})$ s. The observed spotting ignition limits are controlled by the mixing period for the hot moving particle. Thus, the ignition time decreases with higher airflow velocity, agreeing with the experimental results of the Smothering Regime in Fig. 6. The results obtained here can be extrapolated and applied to other forms of the hot ignition source, for example, substituting the estimated *Nu* in Eq. (4) by the variable convection heat transfer corrections for external flow [44].

With a continuous increase of the airflow velocity, this sufficient oxygen supply does not affect the hot particle ignition. While, the thermal conduction within the fuel, mainly reflected in pyrolysate and pyrolysis time, starts to dominate the ignition delay time as

$$t_{py} \approx k_s \rho_s c_s \left(\frac{T_{py} - T_\infty}{\dot{q}_p''} \right)^2 \propto \frac{1}{\dot{q}_p''^2} \tag{5}$$

where $k_s\rho_s c_s$ is the thermal inertia of the fuel, and $\dot{q}_p''$ represents the heat flux from the particle to the fuel. Therefore, the Thermal-Regime ignition delay time remains stable, and exhibits insensitive to the change of airflow velocity, as expressed in Eq. (5) and Fig. 6.

Further increasing the airflow velocity, the wake flow increases the effective heating region. From the experimental results, the chemical duration for the piloted ignition of a flammable mixture will be prolonged. The chemical kinetic-affected ignition can be characterized by a critical Damköhler number (*Da*) when the flow residence time scale (t_{fl}) is close to the chemical reaction time scale (t_{ch}) as

$$Da = \frac{t_{\mathrm{fl}}}{t_{\mathrm{ch}}} = Y_{O_2} Y_F \frac{\alpha_{\mathrm{g}} \rho_{\mathrm{g}}}{U^2} A \exp\left(-\frac{E}{R T_{\mathrm{ig}}} \right) \tag{6}$$

where Y_{O_2} and Y_F are the mass fraction of oxygen and fuel, respectively; α_{g}, ρ_{g} and U are the diffusivity, density, and velocity of airflow, respectively; A and E are the pre-exponential factors, and activation energy of 1-step global chemistry, respectively; R is the universal gas constant; and T_{ig} is the ignition temperature. When the airflow velocity increases, the chemical reaction is difficult to induce, considering the following effects

(1) blown away of combustible gas,
(2) dilution with the excess air,
(3) reduced heterogeneous oxidation,
(4) enhanced heat loss from the reaction.

Herein, the diffusion or flow residence time decreases to be comparable with the chemical time, resulting in the occurrence of no ignition. This airflow velocity is referred to as the critical value for no ignition, which has been obtained by the experimental results in Figs. 3 and 6. The complex airflow effect on hot-particle ignition is difficult to be quantitatively reported by the theoretical study, thus deserves a dedicated investigation in future work.

4.2. Wind effect on the cooling time

Overall, the wind will cool the particle before it hits the fuel or when it rolls horizontally on the fuel bed. To further explain the cooling effect of wind on the hot particle ignition, the cooling time from its initial temperature (T_{p}) to the minimum pilot temperature can be estimated as

$$\rho V c_{\mathrm{p}} \left(T_{\mathrm{p}} - T_{\min} \right) \approx A h \left(T_{\mathrm{p}} - T_{\mathrm{a}} \right) t_{\mathrm{c}} \tag{7}$$

where h is the overall heat transfer coefficient by the fuel bed and the environment, and c_p is the specific heat of the particle. Here minimum piloted temperature should be 850 °C for 16 mm particles and 970 °C for 8 mm particles, respectively. The cooling or effective piloted time of the particle is

$$t_{\mathrm{c}} \approx \frac{\rho_{\mathrm{s}} c_{\mathrm{p}}}{6h \left(T_{\mathrm{p}} - T_{\mathrm{a}} \right)} (1 - e) \left(T_{\mathrm{p}} - T_{\min} \right) D \tag{8}$$

which increases as the particle size and temperature increase. To evaluate the particle temperature, regardless of particle energy effect on the hot-particle ignition, the cooling time of the particles ($T_p = 880$ °C, $D = 16$ mm, and $e = 0.80$) and the particles ($T_p = 940$ °C, $D = 16$ mm, and $e = 0.80$) to 850 °C will be 540 - 400 ms, 1340 - 1000 ms for 0 - 4 m/s airflow velocity, respectively.

Previously, we found that the hot-particle ignition could only take place on the sample surface, and the residence duration of the particle decreased as the particle temperature and moving speed of the particle increased. By frame-by-frame approach to the experimental video, the residence time (t_r) of particle will be 540 ± 10 ms (for $D = 16$ mm, $T_p = 880$ °C and $e = 0.80$ particle) and 500 ± 10 ms (for $D = 16$ mm, $T_p = 940$ °C and $e = 0.80$ particle).

Thus, if the residence time is near the cooling time, the cooling of the wind will affect the hot-particle piloted ignition. This can be confirmed by the flash ignition probability of the particle (for $D = 16$ mm, $T_p = 880$ °C and $e = 0.80$ or solid) decreases as the airflow velocity increases in Fig. 7c. And if the residence time does not exceed the cooling time, the hot particle is sufficient to be a pilot source and the cooling of the wind has a negligible effect on the hot-particle ignition, even during embedding into the EPS foam as shown in Fig. 8.

5. Conclusions

In the work, the limiting conditions for piloted ignition (flash point) and sustained ignition (fire point) by a hot particle have been investigated for the normal and flame-retardant (FR) expandable polystyrene (EPS) foam under an external airflow. Herein, a hot steel spherical particle was dropped onto the low-density normal and FR EPS fuel bed with external airflows of 0-4 m/s. Airflow provides an alternative shortcut transition of unstable flash flame to a strong fire point and burn out the fuel, because airflow increases the oxygen supply and flame heating rather than cooling the particle. As the airflow velocity increases, both flash and fire points first become easier to reach because airflow facilitates the mixing of pyrolysates and oxygen in the Smothering Regime. When the airflow velocity increases to the Thermal Regime, the ignition time remains stable. Further increasing the airflow velocity to the Chemical Regime, the ignition time slightly increases until the wind blows off the flash flame by cooling the particle or blowing away the flammable mixture from the hot surface. Such a competitive effect of wind on hot particle ignition is also qualitatively verified by theoretical analysis. Flame retardants inside EPS foam do not change the flash ignition but inhibit the transition to fire point and burnout, even under the assistance of airflow. This is the first study of the hot-particle ignition of building insulation under windy conditions, helping to enhance the comprehension of the complex interactions between flash points and fire points in the spotting or hot-particle ignition of the building facades.

Credit author statement

Supan Wang: Conceptualization, Investigation, Methodology, Writing - Original Draft, Formal analysis; Funding acquisition. **Chunyin Zhang:** Data curation, Investigation, Writing - Original Draft, Formal analysis. **Kaifeng Wang:** Investigation, Resources. **Xinyan Huang:** Formal analysis, Supervision, Writing - Review & Editing.

Declaration of competing interest

The authors declare that they have no known competing financial interests or personal relationships that could have appeared to influence the work reported in this paper.

Data availability

Data will be made available on request.

Acknowledgements

The research is funded by National Natural Science Foundation of China (NSFC) No. 52176113, University Natural Science Research Project in Jiangsu Province No. 21KJA620003, and Postgraduate Research & Practice Innovation Program of Jiangsu Province No. KYCX21_1194.

Appendix

The dynamic thermal analysis of normal and FR EPS samples was implemented by a TA Instruments simultaneous analyser (SDT-Q600), to obtain the mass loss at a heating rate of 5, 10, 20, and 30 K/min under air atmospheres. At first, the raw fuel was ground into particles, and the initial mass of the sample subjected to the experiments was about 3 mg. There is good repeatability by at least two repeating runs for the given experimental condition. Mass-loss rate of the samples is presented in Fig. A1. The mass loss rate of normal and FR samples rapidly increases at 280 and 250 °C respectively, which is independent of the heating rate indicating the better thermal stability of normal and FR samples.

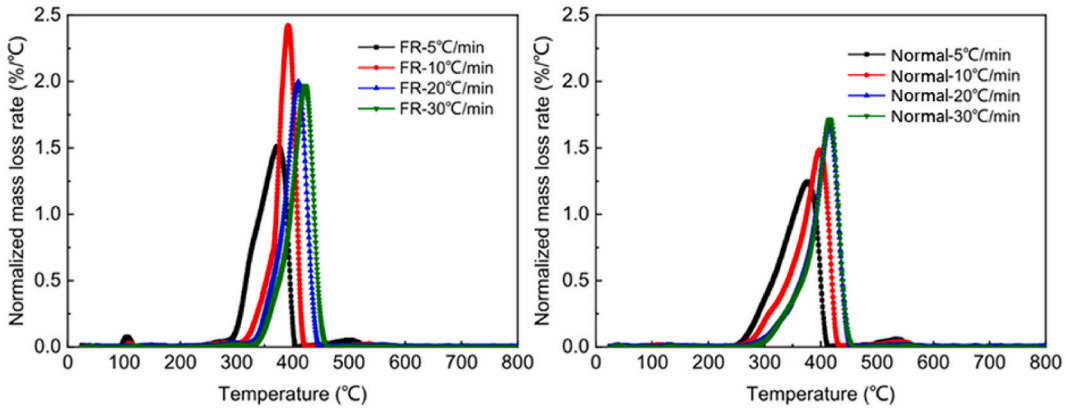

Fig. A1. DTG curves of normal and FR EPS foam at different heating rates.

References

[1] A.M. Papadopoulos, State of the art in thermal insulation materials and aims for future developments, Energy Build. 37 (2005) 77–86.
[2] M.S. McLaggan, J.P. Hidalgo, J. Carrascal, M.T. Heitzmann, A.F. Osorio, J.L. Torero, Flammability trends for a comprehensive array of cladding materials, Fire Saf. J. 120 (2021), https://doi.org/10.1016/j.firesaf.2020.103133.
[3] J. Schulz, D. Kent, T. Crimi, J.L.D. Glockling, T.R. Hull, A critical appraisal of the UK's regulatory regime for combustible façades, Fire Technol. 57 (2021) 261–290, https://doi.org/10.1007/s10694-020-00993-z.
[4] E. Guillaume, V. Dréan, B. Girardin, F. Benameur, T. Fateh, Reconstruction of Grenfell Tower fire. Part 1: lessons from observations and determination of work hypotheses, Fire Mater. 44 (2020) 3–14, https://doi.org/10.1002/fam.2766.
[5] J. Sun, L. Hu, Y. Zhang, A review on research of fire dynamics in high-rise buildings, Theor. Appl. Mech. Lett. 3 (2013), 042001, https://doi.org/10.1063/2.1304201.
[6] S. Wang, H. Chen, N. Liu, Ignition of expandable polystyrene foam by a hot particle: an experimental and numerical study, J. Hazard Mater. 283 (2015) 536–543, https://doi.org/10.1016/j.jhazmat.2014.09.033.
[7] S. Wang, X. Huang, H. Chen, N. Liu, G. Rein, Ignition of low-density expandable polystyrene foam by a hot particle, Combust. Flame 162 (2015) 4112–4118, https://doi.org/10.1016/j.combustflame.2015.08.017.
[8] S. Wang, Y. Zhang, X. Huang, Ignition of EPS foam by a hot moving hollow particle: threshold, auto-ignition, and fire point, Combust. Flame 232 (2021), 111524, https://doi.org/10.1016/j.combustflame.2021.111524.
[9] S.L. Manzello, S. Suzuki, M.J. Gollner, A.C. Fernandez-Pello, Role of firebrand combustion in large outdoor fire spread, Prog. Energy Combust. Sci. 76 (2020), 100801, https://doi.org/10.1016/j.pecs.2019.100801.
[10] J. Song, S. Wang, H. Chen, Safety distance for preventing hot particle ignition of building insulation materials, Theor. Appl. Mech. Lett. 4 (2014), 034005, https://doi.org/10.1063/2.1403405.
[11] H. Xu, K. Lin, S. Mao, J. Wang, Y. Ding, K. Lu, Numerical investigation of air curtain jet effect upon the compartment-facade fire safety protection based on temperature evolution and thermal impact, Therm. Sci. Eng. Prog. (2023), 101988, https://doi.org/10.1016/j.tsep.2023.101988.
[12] A.C. Fernandez-Pello, Wildland fire spot ignition by sparks and firebrands, Fire Saf. J. 91 (2017) 2–10, https://doi.org/10.1016/j.firesaf.2017.04.040.
[13] J. Quintiere, Fundamentals of Fire Phenomena, John Wiley & Sons, Ltd, London, 2006, https://doi.org/10.1002/0470091150.
[14] S.E. Caton, R.S.P. Hakes, D.J. Gorham, A. Zhou, M.J. Gollner, Review of pathways for building fire spread in the wildland urban interface Part I: exposure conditions, Fire Technol. 53 (2017) 429–473, https://doi.org/10.1007/s10694-016-0589-z.
[15] W. Fang, Z. Peng, H. Chen, Ignition of pine needle fuel bed by the coupled effects of a hot metal particle and thermal radiation, Proc. Combust. Inst. (2021) 5101–5108, https://doi.org/10.1016/j.proci.2020.05.032.
[16] C. Lautenberger, C. Fernandez-Pello, A model for the oxidative pyrolysis of wood, Combust. Flame 156 (2009) 1503–1513, https://doi.org/10.1016/j.combustflame.2009.04.001.
[17] Y. Liu, J.L. Urban, C. Xu, C. Fernandez-Pello, Temperature and motion tracking of metal spark sprays, Fire Technol. 55 (2019) 2143–2169, https://doi.org/10.1007/s10694-019-00847-3.
[18] J.L. Urban, C.D. Zak, J. Song, C. Fernandez-Pello, Smoldering spot ignition of natural fuels by a hot metal particle, Proc. Combust. Inst. 36 (2017) 3211–3218, https://doi.org/10.1016/j.proci.2016.09.014.
[19] J.L. Urban, C.D. Zak, C. Fernandez-Pello, Spot fire ignition of natural fuels by hot aluminum particles, Fire Technol. 54 (2018) 797–808, https://doi.org/10.1007/s10694-018-0712-4.
[20] P. Yin, N. Liu, H. Chen, J.S. Lozano, Y. Shan, New correlation between ignition time and moisture content for pine needles attacked by firebrands, Fire Technol. 50 (2014) 79–91, https://doi.org/10.1007/s10694-012-0272-y.
[21] R.M. Hadden, S. Scott, C. Lautenberger, C.C. Fernandez-Pello, Ignition of combustible fuel beds by hot particles: an experimental and theoretical study, Fire Technol. 47 (2011) 341–355, https://doi.org/10.1007/s10694-010-0181-x.
[22] W. Yang, Z. Tao, R. Yang, Z. Gao, J. Wang, Study on the mechanism of molten aluminum droplets igniting EPS foam, Combust. Flame 244 (2022), 112297, https://doi.org/10.1016/j.combustflame.2022.112297.
[23] S. Wang, X. Huang, H. Chen, N. Liu, Interaction between flaming and smouldering in hot-particle ignition of forest fuels and effects of moisture and wind, Int. J. Wildland Fire 26 (2017) 71–81, https://doi.org/10.1071/WF16096.
[24] P.F.M. Ellis, Fuelbed ignition potential and bark morphology explain the notoriety of the eucalypt messmate "stringybark" for intense spotting, Int. J. Wildland Fire 20 (2011) 897–907, https://doi.org/10.1071/WF10052.
[25] P.F.M. Ellis, The effect of the aerodynamic behaviour of flakes of jarrah and karri bark on their potential as firebrands, J. Roy. Soc. West Aust. 93 (2010) 21–27.
[26] D. Rich, C. Lautenberger, J.L. Torero, J.G. Quintiere, C. Fernandez-Pello, Mass flux of combustible solids at piloted ignition, Proc. Combust. Inst. 31 (2007) 2653–2660, https://doi.org/10.1016/j.proci.2006.08.055.
[27] D.X. Viegas, M. Almeida, J. Raposo, R. Oliveira, C.X. Viegas, Ignition of mediterranean fuel beds by several types of firebrands, Fire Technol. 50 (2014) 61–77, https://doi.org/10.1007/s10694-012-0267-8.
[28] S.L. Manzello, T.G. Cleary, J.R. Shields, A. Maranghides, W. Mell, J.C. Yang, Experimental investigation of firebrands: generation and ignition of fuel beds, Fire Saf. J. 43 (2008) 226–233, https://doi.org/10.1016/j.firesaf.2006.06.010.

[29] S.L. Manzello, S.-H. Park, T.G. Cleary, Investigation on the ability of glowing firebrands deposited within crevices to ignite common building materials, Fire Saf. J. 44 (2009) 894–900, https://doi.org/10.1016/j.firesaf.2009.05.001.
[30] S.L. Manzello, Y. Hayashi, T. Yoneki, Y. Yamamoto, Quantifying the vulnerabilities of ceramic tile roofing assemblies to ignition during a firebrand attack, Fire Saf. J. 45 (2010) 35–43, https://doi.org/10.1016/j.firesaf.2009.09.002.
[31] S. Suzuki, E. Johnsson, A. Maranghides, S.L. Manzello, Ignition of wood fencing assemblies exposed to continuous wind-driven firebrand showers, Fire Technol. 52 (2016) 1051–1067, https://doi.org/10.1007/s10694-015-0520-z.
[32] P.F.M. Ellis, P.F.M. Ellis, The likelihood of ignition of dry-eucalypt forest litter by firebrands, Int. J. Wildland Fire 24 (2015) 225–235, https://doi.org/10.1071/WF14048.
[33] A. Ganteaume, C. Lampin-Maillet, M. Guijarro, C. Hernando, M. Jappiot, T. Fonturbel, P. Pérez-Gorostiaga, J.A. Vega, A. Ganteaume, C. Lampin-Maillet, M. Guijarro, C. Hernando, M. Jappiot, T. Fonturbel, P. Pérez-Gorostiaga, J.A. Vega, Spot fires: fuel bed flammability and capability of firebrands to ignite fuel beds, Int. J. Wildland Fire 18 (2009) 951–969, https://doi.org/10.1071/WF07111.
[34] X. Huang, J. Zhao, Y. Zhang, Y. Zhou, Q. Wang, J. Sun, Effects of altitude and sample orientation on heat transfer for flame spread over polystyrene foams, J. Therm. Anal. Calorim. 121 (2015) 641–650, https://doi.org/10.1007/S10973-015-4615-Z/FIGURES/11.
[35] Y. Huang, L. Hu, Y. Ma, N. Zhu, Y. Chen, J. Wahlqvist, M. Mcnamee, P. van Hees, Experimental study of flame spread over thermally-thin inclined fuel surface and controlling heat transfer mechanism under concurrent wind, Int. J. Therm. Sci. 165 (2021), 106936, https://doi.org/10.1016/J.IJTHERMALSCI.2021.106936.
[36] D. Rich, C. Lautenberger, J.L. Torero, J.G. Quintiere, C. Fernandez-Pello, Mass flux of combustible solids at piloted ignition, Proc. Combust. Inst. (2007), https://doi.org/10.1016/j.proci.2006.08.055.
[37] M.A. Santoso, E.G. Christensen, J. Yang, G. Rein, Review of the transition from smouldering to flaming combustion in wildfires, Front. Mech. Eng. 5 (2019) 1–20, https://doi.org/10.3389/fmech.2019.00049.
[38] M. Rossi, G. Camino, M.P. Luda, Characterisation of smoke in expanded polystyrene combustion, Polym. Degrad. Stabil. 74 (2001) 507–512, https://doi.org/10.1016/S0141-3910(01)00168-9.
[39] W. An, L. Jiang, J. Sun, K.M. Liew, Correlation analysis of sample thickness, heat flux, and cone calorimetry test data of polystyrene foam, J. Therm. Anal. Calorim. 119 (2015) 229–238, https://doi.org/10.1007/S10973-014-4165-9/FIGURES/10.
[40] S.T. McKenna, N. Jones, G. Peck, K. Dickens, W. Pawelec, S. Oradei, S. Harris, A.A. Stec, T.R. Hull, Fire behaviour of modern façade materials – understanding the Grenfell Tower fire, J. Hazard Mater. 368 (2019) 115–123, https://doi.org/10.1016/j.jhazmat.2018.12.077.
[41] O.M. Putzeys, A.C. Fernandez-Pello, G. Rein, D.L. Urban, The piloted transition to flaming in smoldering fire retarded and non-fire retarded polyurethane foam, Fire Mater. 32 (2008) 485–499, https://doi.org/10.1002/fam.981.
[42] C.Y.H. Chao, J.H. Wang, Transition from smoldering to flaming combustion of horizontally oriented flexible polyurethane foam with natural convection, Combust. Flame 127 (2001) 2252–2264, https://doi.org/10.1016/S0010-2180(01)00326-1.
[43] A. Gossiaux, P. Bachelet, S. Bellayer, S. Ortgies, A. König, S. Duquesne, Small-scale single burning item test for the study of the fire behavior of building materials, Fire Saf. J. 125 (2021), 103429, https://doi.org/10.1016/j.firesaf.2021.103429.
[44] T.L. Bergman, T.L. Bergman, F.P. Incropera, D.P. Dewitt, A.S. Lavine, Fundamentals of Heat and Mass Transfer, John Wiley & Sons, 2011.
[45] J. Gong, M. Zhang, Y. Jiang, C. Zhai, Z. Wang, Limiting condition for auto-ignition of finite thick PMMA in forced convective airflow, Int. J. Therm. Sci. 161 (2021), 106741, https://doi.org/10.1016/j.ijthermalsci.2020.106741.
[46] J. Gong, L. Yang, A Review on Flaming Ignition of Solid Combustibles: Pyrolysis Kinetics, Experimental Methods and Modelling, Fire Technol, 2022, https://doi.org/10.1007/s10694-022-01339-7.
[47] S. McAllister, C. Fernandez-Pello, D. Urban, G. Ruff, The combined effect of pressure and oxygen concentration on piloted ignition of a solid combustible, Combust. Flame 157 (2010) 1753–1759, https://doi.org/10.1016/j.combustflame.2010.02.022.
[48] M. Thomsen, C. Fernandez-Pello, S.L. Olson, P.V. Ferkul, Downward burning of PMMA cylinders: the effect of pressure and oxygen, Proc. Combust. Inst. (2021), https://doi.org/10.1016/j.proci.2020.05.024.
[49] A.C. Fernandez-Pello, S.R. Ray, I. Glassman, Flame spread in an opposed forced flow: the effect of ambient oxygen concentration, Symp. Combust. (1981), https://doi.org/10.1016/S0082-0784(81)80063-X.
[50] X. Huang, J. Gao, A review of near-limit opposed fire spread, Fire Saf. J. 120 (2021), 103141, https://doi.org/10.1016/j.firesaf.2020.103141.
[51] J.G. Quintiere, Fundamentals of Fire Phenomena, 2006, https://doi.org/10.1002/0470091150.
[52] G. Wang, X. Chen, P. Liu, S. Bai, Flame-retardant mechanism of expandable polystyrene foam with a macromolecular nitrogen–phosphorus intumescent flame retardant, J. Appl. Polym. Sci. 134 (2017).